Journal of Thermal Analysis and Calorimetry (2019) 135:73–82
https://doi.org/10.1007/s10973-017-6946-4

Experimental study on the effect of copper oxide nanoparticles on thermophysical properties of ethylene glycol–water for using in indirect heater at city gate stations

A. R. Rahmati[1] · M. Reiszadeh[1]

Received: 17 September 2017 / Accepted: 3 December 2017 / Published online: 9 January 2018

Abstract

This study aimed to investigate the increase in heat transfer in the indirect heater at a city gate station (CGS) with the addition of copper oxide (CuO) nanoparticles to water–ethylene glycol base fluids. Indirect heaters are typically used at CGSs to raise the heat transfer coefficient of output gas flow from − 5 to 15 °C. Moreover, manufacturing laboratory equipment in the presence of water–ethylene glycol base fluid and the nanoparticle in volume fractions of 0.05, 0.1, 0.2, and 0.3 at a temperature of 40–70 °C was discussed using dimensional simulation and analysis. The physical properties of the base fluid and nanofluid were measured using precise devices. Heat transfer tests for the base and nanofluid, as well as replacing of the air by gas, were conducted in a simulated and developed device. According to the obtained results with respect to the changes in convection and conduction heat transfer, enhancement of temperature difference at a rate of 36% was observed in the indirect heater with nanoparticle volume concentration of 0.2% at a temperature of 70 °C. Moreover, the Nusselt number showed a relatively good agreement with theoretical discussions.

Keywords Copper oxide nanofluid · Heat transfer · Indirect heater · Gas compressibility fluid · Air

List of symbols

A	Cross-sectional area (m^2)
C_p	Specific heat (J kg^{-1} K^{-1})
D	Pipe diameter (m)
H	Heat transfer coefficient (W m^{-2} K^{-1})
K	Thermal conductivity (W m^{-1} K^{-1})
L_p	Nanotube length (m)
L	Length of test tube (m)
Nu	Nusselt number
P	Pressure (Pa)
Re	Reynolds number
T	Temperature (K)
U	Velocity vector (m s^{-1})
V	Volume (m^3)
Pr	Prandtl number
T_m	Mean temperature (K)
$\dot{m}$	Mass rate (kg s^{-1})

Subscript

bf	Base fluid
P	Nanoparticle
i	Inlet
O	Outlet
Exp	Experimental
C	Cold fluid
H	Hot fluid
nf	Nanofluid
m	Average
EG	Ethylene glycol
W	Water
CuO	Copper oxide

Greek symbols

ΔP	Pressure drop (P)a
ρ	Density (kg m^{-3})
μ	Dynamic viscosity (kg m^{-1} s^{-1})
φ	Volume fraction

✉ A. R. Rahmati
ar_rahmati@kashanu.ac.ir

[1] Department of Mechanical Engineering, University of Kashan, Kashan 87317-51167, Iran

Introduction

Town border stations (TBS) reduce the high pressure due to gas movement from the refinery to the consumption points inside the town. One of the most important parts of city gate station (CGS) is their preheating system. Hence, an indirect heating was used to supply the needed energy from high-quality refined gas. Heaters in natural gas gate stations as energy equipment in gas delivery industry are used in many countries including Iran. One of the main problems of these preheating systems is the low efficiency that causes high energy waste.

Therefore, improving the efficiency of these indirect heaters will have considerable implications for the consumption of natural gas. Owing to the high pressure of natural gas at the consumption points, the pressure should be reduced before consumption. This pressure reduction occurs at the CGSs. Pressure at CGSs is usually reduced to 1.5–2 MPa [1]. For positive Joule–Thomson effect on natural gas, pressure reduction leads to a drop in the natural gas temperature; the value of natural gas temperature should not be less than the minimum allowed value.

This temperature, called the temperature of hydrate formation, depends on the pressure and composition of natural gas. In fact, freezing water droplets suspended in natural gas occur in the hydrate formation area, blocking the pipeline transmission, especially in cold seasons. To prevent hydrate formation, natural gas flow should be heated up to a specific level before pressure reduction.

In general, line heaters in CGSs are used for preheating the natural gas flow with a lot of fuel consumption to supply the required heat. For this reason, the efficiency of CGSs is not at a satisfactory level. Not many studies have been carried out on the efficiency improvement in CGSs using combined cogeneration of heat, electricity, and expander turbines [2, 3]. One of such studies presents a new configuration, namely nanotechnology, to reduce fuel consumption at CGSs.

Nanofluid was used for the first time by Choi [4]. Subsequently, a lot of research was done to show nanofluids have a good potential for heat transfer applications [5–20]. Xuan and Li [21] experimentally investigated the convention heat transfer coefficient of nanofluid containing copper nanoparticles in laminar and turbulent flow in the tube. According to the their results, the heat transfer coefficient of nanofluid is greater than base fluid and the heat transfer process of nanofluid increases drastically with enhanced composition of nanoparticles. The dispersion of nanoparticles and the method for preparing fluids are important parameters for improving the efficiency of nanoparticles. Li and Xuan [22] observed higher Reynolds number and consequently a significant growth in the convention heat transfer coefficient of nanofluid than water at a volume concentration of 2% of water and copper oxide nanofluid. Base nanofluid ethylene glycol has been enhanced up to 35% with addition of 2% volume of copper oxide.

Farzaneh Gord et al. [23] conducted the first study on the effects of flat solar collectors on the supply of the required heat at CGSs. Farzaneh Gord et al. [24] attempted to install solar systems in Sari City, Iran, and presented a solar system to store the required heat by the solar collector and hot water storage during the day and use it overnight. The system consists of an array of 450 solar collectors, and the storage tank has a capacity of 45 cubic meters, which can store fuel consumption up to 11.3%. They changed the above system by including a further storage tank in the second study. Storage tanks in this configuration would collect the sun's heat during the day and return to the heater at night, when more heat is needed. As a result, fuel consumption has been decreased by 14%, while in the first system only 11% reduction was observed. In the third study, Farzaneh Gord et al. [25] replaced the conventional linear heater at CGSs with an automatic controllable heater and compared the thermal behavior in this system with the mentioned systems. The result of this comparison shows the superiority of the last system in the two previous cases. In a new study conducted by Behseresht et al. [26], the migration effects of nanoparticles addressed by other researchers were discussed and the improper selection of dimensionless number range in previous studies was revealed. Regarding the proper range of dimensionless number, heat transfer is negligible due to the migration of nanoparticles. In another study, Noghreh Abadi et al. [27] showed that, although heat transfer caused by the migration of nanoparticles is negligible, nanoparticle slip in base fluid causes heterogeneity in the nanofluid. This heterogeneity changed the structural characteristics of Nanofluid, thereby affecting the convention heat transfer in nanofluids. Hossein et al. [28], in a numerical study on heat transfer and friction in an elliptical tube, with the addition of 0.25 and 1% volume of nano-titanium oxide with a diameter of 27–50 nm of particles, found an increase in heat transfer at a rate of 9% and friction coefficient at a rate of 6% compared to circular tubes. According to a study by Mahmoud et al. [29], the surface tension and heat transfer in static ethylene glycol fluid using iron oxide nanoparticles possess greater Nusselt number than water-based fluid. Despite sophisticated developments in the field of nanotechnology, the application of copper oxide nanoparticles in indirect heaters at CGSs has not been studied. This is the first research on the enhancement of heat transfer in indirect heaters at a CGS and the shortening of heater size and reduction in fuel consumption.

Indirect heaters at city gate stations

In winter, gas freezing occurs at CGSs due to pressure drop, blocking the gas passage. To prevent this, heaters are necessary to supply the required gas before gas pressure reduction [30].

During heating, direct heat transfer should not occur in the exchangers for reasons of safety. Water as a medium fluid should transfer the heat from the heating source to the gas pipe, and ethylene glycol is added to the water to prevent freezing in winter.

The reason for pressure reduction in the entrance pipe in cities is that after extraction gas is transmitted to the urban consumer with pressure of 1000 psi. This pressure is very high to be used by the consumer. Therefore, the gas pressure is reduced from 1000 psi to 250 psi at CGSs with the valve of a pressure regulator. Gas in the pipelines is exposed to pressure drop, which reduces the temperature. Owing to pressure reduction and reaching of the gas temperature to the dew point, the gas condensate comprising heavy hydrocarbons changes from the gas state to the liquid state, which turns it into ice in the cold season.

Heaters at CGSs are similar to shell and tube converters, as they are in the form of a horizontal cylindrical source with high volume and the volume is proportional to the thermal capacity of the heater. Pipe size is designed according to the volume of gas passing through the pipes. Gas is passed through these pipes and heated. In the shell part of the heater, there are water, i.e., ethylene glycol solution and fire tube. Water–ethylene glycol solution in the converter is an intermediate to transfer thermal energy from the warm fluid to cold fluid, and heat transfer mechanisms in these converters follow convection heat transfer [31].

There is no external factor in convention heat transfer and fluid motion only due to the influence of density. In convention heat transfer, fluid surrounds the heat source and receives heat. Thus, its density is lowered and replaced with cold fluid, and it is then heated and the cycle continues. This process transfers thermal energy from the hot fluid to the gas-passing pipe. Convection is a mechanism or a type of heat transfer where the fluid motion is transferred by the density difference in the fluid that is provided by the temperature gradient. In convection heat transfer, fluid velocity is very low, so the value of heat transfer is also very low [32].

The components of indirect heaters in a gas company (Fig. 1) are as follows:

- Cylindrical shell as the converter container
- Spiral pipes of gas passing into the converter
- Storage or expansion of water source
- Burners
- Chimney
- Fire tube (fire warehouse)
- Controlling systems for conducting the fuel to burners

Description of device testing

The laboratory device made (Fig. 2) for the heater test which is actually a closed-circuit system comprises a compressor, a pressure drop regulator valve, a cooling tank for returned water, accurate instruments such as a barometer, a flow meter, thermocouples, water–ethylene glycol solution, and copper oxide nanoparticles. Air compressor is used to create the necessary pressure instead of gas, and valve regulates the pressure drop. The cooling tank removes the heat of the hot water returned from the heater and transports it to the desired temperature. The flow meter sends the intended rate for testing with regulating the existing valve. In the shell part of the device, there are water–ethylene glycol and nanoparticles. The ratio of water to ethylene glycol is 50:50 at ambient temperature. However, in conducting the test, air is replaced by cold gas and necessary changes are applied regarding the rules of similarity and dimensional analysis [33, 34]. Thermocouples are located for measuring the inlet and outlet temperatures. The nanofluid's motion due to embedded pump prevents the deposition of nanoparticles. In this test, CuO nanofluid is poured in the indirect heaters with fixed water–ethylene glycol base fluid in various concentrations.

Different parts of a laboratory-developed indirect heater are:

- Converter shell
- Converter tube (U-shaped) and inlet and outlet valves
- Pump
- Inlet and outlet pipes of the pump
- Inlet and outlet valves of the pump
- Device discharge valve
- Heating element
- Visiting gate
- Accurate instruments such as a speedometer, barometer, and thermometer

A converter shell is a 15-L cylinder made of steel sheet with a diameter of 300 mm and a length of 80 cm. Complete specifications of the laboratory-made device are given in Table 1.

On the inlet and outlet surfaces of the pipe in the device, two 0.25-inch valves have been installed to change the amount of airflow at the exit and entrance of the device. The inlet air pressure and outlet air pressure of the device are 1.5 and 1 bar, respectively, and the device is adjusted using installed valves on the input and output surfaces of the pipe. It is noteworthy that the required air that is used as

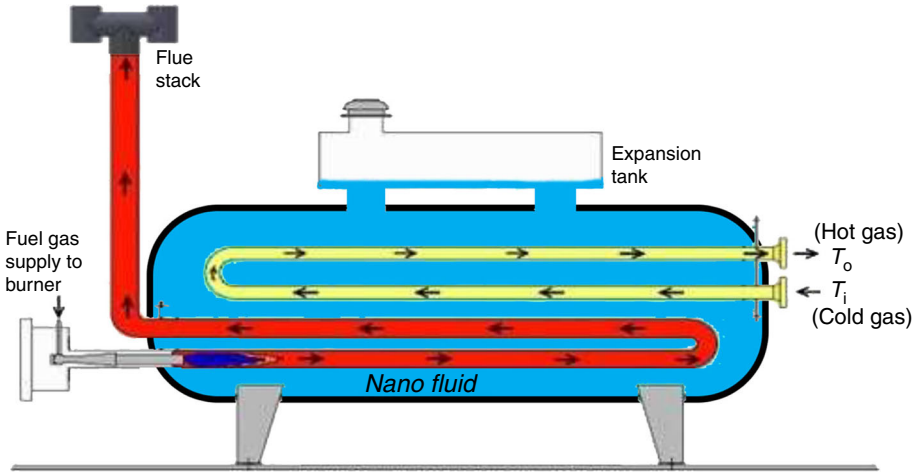

Fig. 1 Total scheme of indirect heater at a city gate station

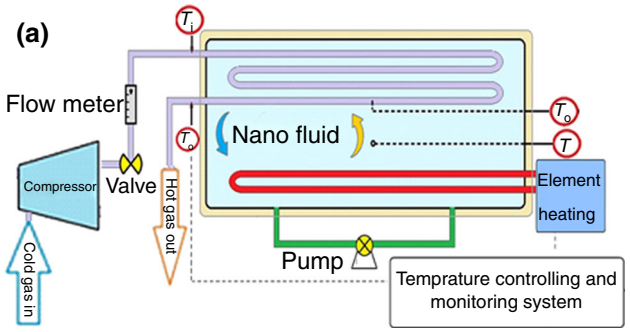

Fig. 2 **a** Scheme of laboratory system. **b** Laboratory-developed indirect heater

Table 1 Specifications of the laboratory-made device

The number of passes—Return converter	6
Outlet diameter/in	0.375
Thickness/mm	0.8
Length of exchanger tube in a single pass/cm	80
Type of converter	Copper oxide

a gas substitute has been provided in the laboratory through a compressor with the pressure of 10 bar. One of the main tasks for the non-settling of the nanoparticles is performed by a pump having the capacity of 0.5 horsepower (SQ660 model), which gets the fluid from the bottom part of the shell and again pumps back to the shell. As seen in the figures, in the input and output parts of the pump, two 1-inch valves are installed. When the pump is not needed, we can close the valves and discharge the nanofluids from the heater tank.

Stabilizing the nanofluids

In this study, copper oxide particles with physical and thermophysical properties have been used as nanoparticles with a diameter of 40 nm and water–ethylene glycol at a ratio of 50:50 has been used as the base fluid (Table 2), while sodium dodecyl sulfate has been used as active surfactant (Table 3) for preparing the nanofluids.

The size of the copper oxide nanofluids was evaluated using SEM and TEM images. As shown in Fig. 3, the copper oxide nanoparticles have a relatively spherical shape and a number of them have an agglomerate shape with an uneven surface. Both images show that the average diameter of particles is less than 100 nm. In order to ensure the stability of the nanofluids and the existence of the functional groups, copper oxide nanofluids have been evaluated using the FTIR spectrum of infrared spectroscopy, as Fig. 4 shows.

The concentration change in the surfactant and its effect on nanofluid sustainability, as well as the concentration of surfactant, sodium dodecyl sulfate used in nanofluids, and optimal weight conditions of 0.1% by PH = 7.8 have been selected. According to Fig. 5, the optimum conditions of the nanofluids are kept stable for at least 27 days; however, in the indirect heater system, they are circulated by a nanofluid pump and nanoparticle sedimentation is minimized.

Table 2 Physical properties of base fluid, air, and nanoparticles at ambient temperature

Material	Density ρ/kg m^{-3}	Viscosity μ/m Pas	Specific heat Cp/J kg^{-1} K^{-1}	Thermal conductivity K/W m^{-1} K^{-1}
EG/W (50:50)	1059	2.94	3468	0.404
Air	1.1839	1.8×10^{-5}	1007	0.02551
CuO (40 nm)	6320	–	531.02	400

Table 3 Specification of surfactant

Surfactant	Molecular formula	Molecular weight/g Mol^{-1}	Density/g cm^{-3}
Sodium dodecyl sulfate	NAC12H25SO4	288.372	1.01

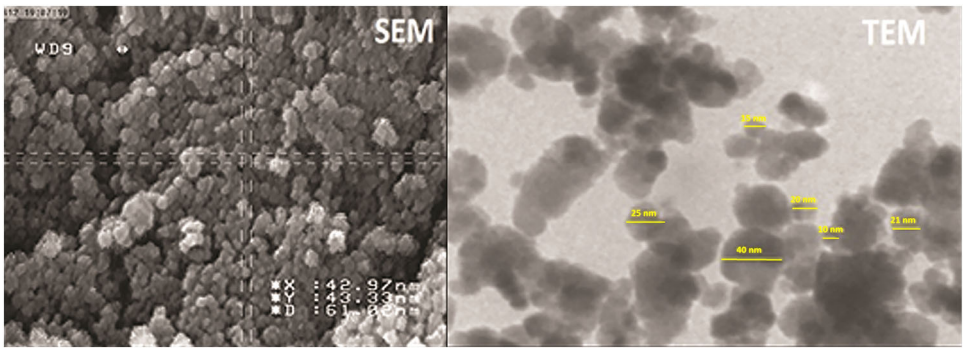

Fig. 3 SEM and TEM images of copper oxide nanofluids

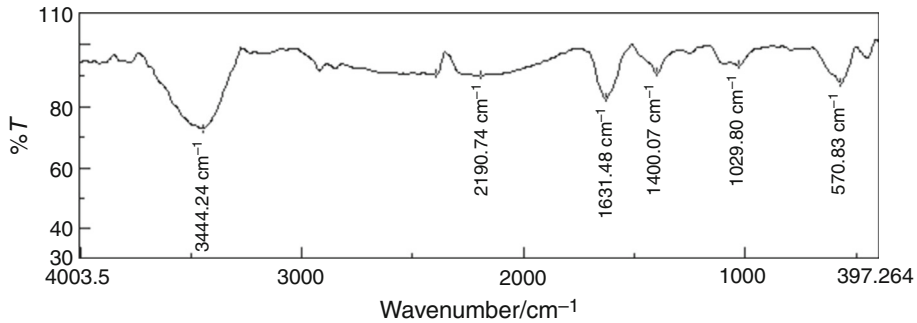

Fig. 4 FTIR spectrum of copper oxide nanofluids

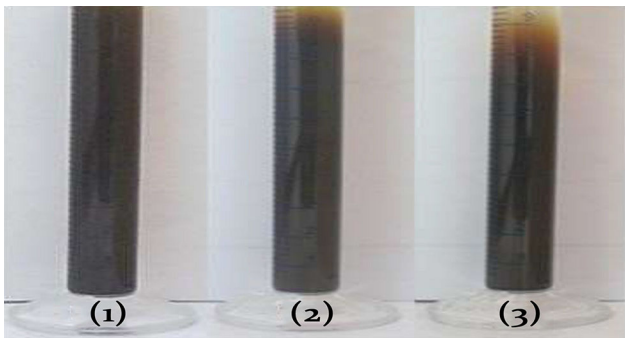

Fig. 5 Stability of nanoparticles in the base fluid. 1. After 7 days, 2. after 15 days, and 3. after 27 days

Equations and calculations

To develop laboratory equipment, dimensionless quantity needs to be calculated [17, 18] using

$$\text{Dimensionless length} = \frac{L}{D}, \quad \text{Dimensionless pressure} = \frac{\Delta P}{\rho v^2}, \quad Re = \frac{\rho v D}{\mu}. \tag{1}$$

dimensional and similarity analysis in the following manner.

In the above equations, L represents the length of the tube, D is the diameter of the inlet and outlet of the gas pipe, V is airflow velocity, μ is the viscosity of air, ρ is the density of air, and ΔP represents the air pressure

difference. Convection heat transfer coefficient is defined using Eq. (2)

$$H = \frac{m\, cp\left(\dot{T} - T_1\right)}{A(T_W - T_m)}, \tag{2}$$

In this equation, m is the mass rate of the entered air and C_P is specific heat, T_0 and T_i are inlet and outlet air temperatures, respectively, and A is the lateral surface of the pipe. In order to calculate the properties of the base fluid in the indirect heater tank, the equations of density, viscosity, specific heat, and base fluid conductivity coefficient, i.e., the identical mixture of water and ethylene glycol (50:50) at different temperatures derived by Eqs. (3)–(6), have been used [35, 36].

$$\rho_{bf} = -0.002475T^2 + 0.9998T + 1002.5, \tag{3}$$

$$\mu_{bf} = 0.001 \times \exp\left(3135.6 \times \frac{1}{T} - 8.9367\right), \tag{4}$$

$$C_{Pbf} = 4.248T + 1882.4, \tag{5}$$

$$K_{bf} = -0.1054 + 0.0025T - 3.196 \times 10^{-6} \times T^2. \tag{6}$$

Equations (7)–(9) show how the properties of the copper oxide nanofluid have been calculated. The density and specific heat capacity are calculated using Pak and Cho equations [37]:

Nanofluid viscosity is calculated using the Brinkman equation [38] as follows:

$$\rho_{nf} = (1 - \varphi)\rho_{bf} + \varphi\rho_p, \tag{7}$$

$$c_{p,nf} = \frac{(1 - \varphi)\rho_{bf}C_{p,bf} + \varphi\rho_p C_{p,p}}{\rho_{nf}}, \tag{8}$$

$$\mu_{nf} = \mu_{bf}\frac{\mu_{bf}}{(1 - \varphi)^{2.5}}, \tag{9}$$

Nanofluid thermal conductivity coefficient is obtained using the Yu and Choi equation derived by modified Maxwell's equation [39]:

$$K_{nf} = K_{bf}\left[\frac{K_p + 2K_{bf} - 2\varphi(K_{bf} - K_P)}{K_p + 2K_{bf} - \varphi\left(K_{bf} - K_p\right)}\right]. \tag{10}$$

To calculate Nusselt theory, the Dittos-Bolter Eq. (11) has been used [40].

$$N_u = 0.0243Re^{0.8}Pr^{0.4}. \tag{11}$$

Results and discussion

In this section, the data obtained from the tests are presented in tables and diagrams. First, Table 4 presents the obtained values of indirect heaters in the absence of nanoparticles in water–ethylene glycol base fluid (W/EG) with equal ratio (50:50). In the next steps, copper oxide nanoparticles are added to the base fluid in volume fractions of 0.025, 0.05, 0.1, 0.2, and 0.3, and some changes are created in the nanofluid and air. Consequently, based on these changes, the amount of heat transfer is recorded.

In Figs. 6 and 7, the viscosity of the nanofluid at different temperatures and volume fractions is presented. Comparisons in the diagrams show that the higher the temperature of the nanofluid, the less the viscosity; however, with increasing volume fraction of nanoparticles, the nanofluid's viscosity increases as well. The highest nanofluid viscosity is reached in the highest volume fraction and the lowest temperature in the indirect heater tank.

Figure 8 shows the density of the nanofluid at different temperatures and volume fractions. Comparisons of diagrams show that, with increasing temperature, the density has not changed, but with increasing volume of the nanoparticles, the nanofluid's density has increased. The maximum density in the highest volume fraction and at maximum temperature does not affect the nanofluid's density.

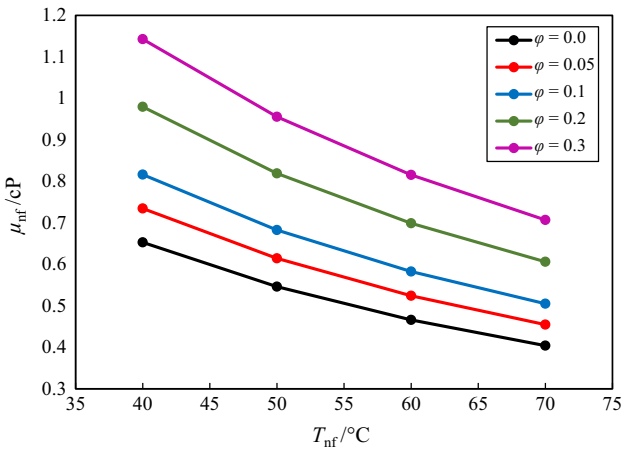

Fig. 6 Viscosity of nanofluids at different temperatures and volume fractions

Table 4 Obtained values for base fluid and air temperature in the laboratory-developed heater

T_{nf}/°C	K/W m^{-1} K^{-1}	ρ_{nf}/kg m^{-3}	μ_{nf}/cP	$C_{p,nf}$/J kg^{-1}	T_i/°C	T_o/°C	ΔT/°C
40	0.3640	1072.9	2.9341	3212.66	28	35.26	7.26
50	0.3687	1067.1	2.1523	3255.14	28.6	41.84	13.24
60	0.3727	1060.9	1.6085	3297.62	28.5	49.06	20.56
70	0.3761	1054.1	1.2226	3340.10	29.5	52.70	23.20

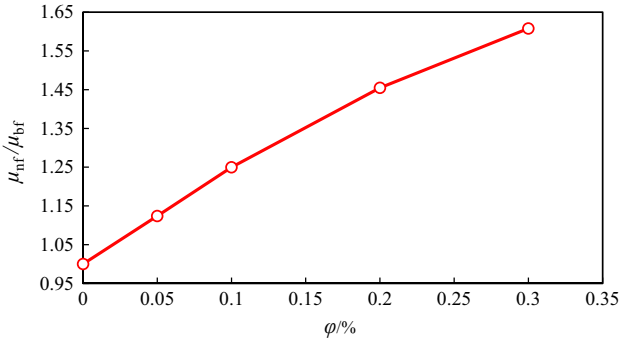

Fig. 7 Ratio of the viscosity of nanofluid to the viscosity of base fluid at different volume fractions of nanoparticles

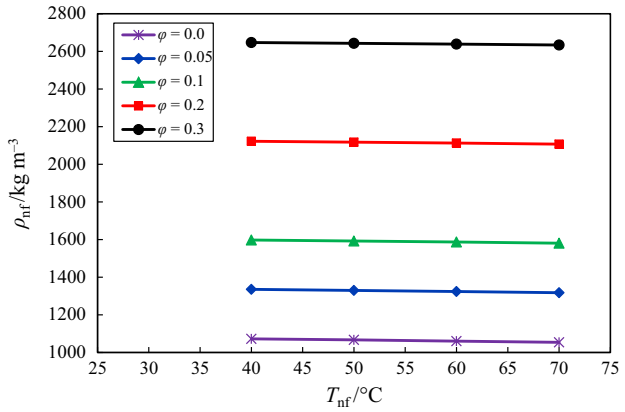

Fig. 8 Density of nanofluids at different temperatures and volume fractions

Figure 9 shows the specific thermal capacity of the nanofluid at different temperatures and volume fractions. The comparisons of diagrams show that higher temperature of the nanofluid does not affect the specific thermal capacity and that with, increasing volume fraction of the nanoparticles, the nanofluid's specific thermal capacity has decreased. Therefore, the maximum specific thermal capacity is observed in the lowest volume fraction.

In Figs. 10 and 11, the temperature difference has been initially increased for the increased volume fraction of the copper oxide nanoparticles at different temperatures of the heater tank. After that, this difference will be higher at the volume fraction of 0.2 and 0.3% with an increase in temperature. At 35 °C above, the highest temperature difference is observed in 0.2% volume fraction, and the results of the present study are consistent with the study of Li and Xuan [22].

As shown in Figs. 12 and 13, increased conductivity coefficient of the nanofluid as a factor in increasing air (gas) transfer in the indirect heater is one of the objectives of this study. This factor increases to 0.2% with a higher volume fraction of the nanoparticles and reaches 33%,

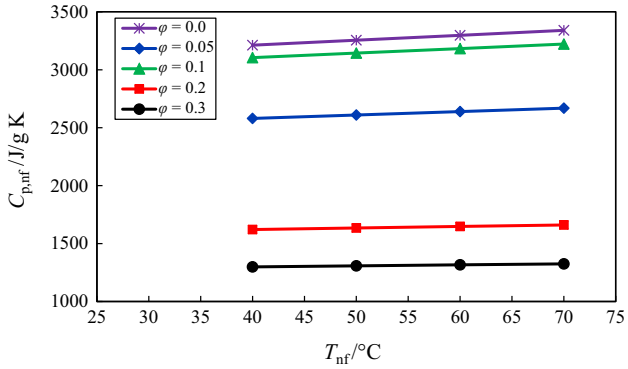

Fig. 9 Specific thermal capacity of nanofluids at different temperatures and volume fractions

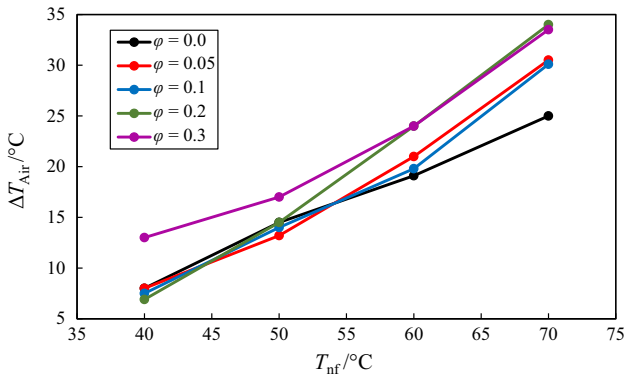

Fig. 10 Difference between inlet and outlet temperatures of air at different temperatures and volume fractions of nanofluids

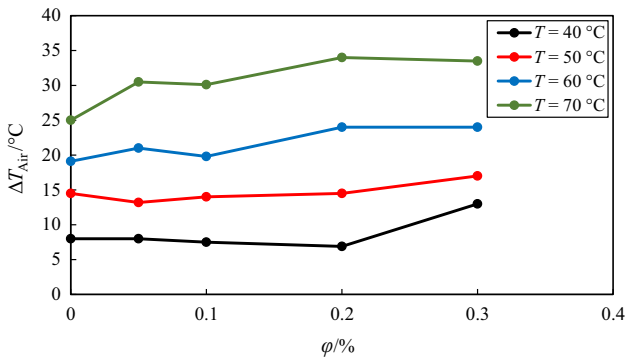

Fig. 11 Obtained air temperature differences at different volume fractions of nanofluids

leading to increased air temperature or outlet gas in the pipe.

The highest temperature difference in volume fraction of 0.2 and tank's temperature of 70 °C was 43 °C, while, the obtained highest temperature difference is equal to 25 °C in the absence of nanoparticles. In other words, the temperature difference has been increasing at a rate of 43%

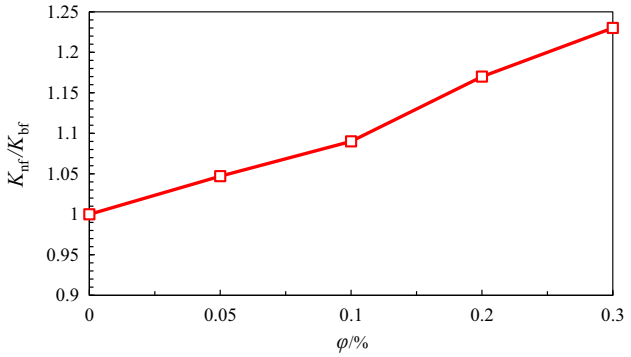

Fig. 12 Thermal conductivity coefficient ratio to copper oxide nanoparticle volume fraction

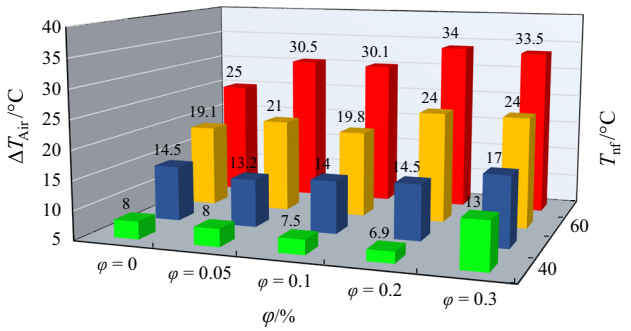

Fig. 13 Nanofluid temperature difference in different volume fractions with increasing temperature in the heater tank

with the addition of 0.2% volume fraction of copper oxide nanoparticles in indirect heater in this experimental study.

$$\left(\frac{\Delta T_{\mathrm{O}} - \Delta T_{\mathrm{i}}}{\Delta T_{\mathrm{i}}}\right) \times 100 \approx 36\% \tag{12}$$

The pump used in the laboratory system for recirculation of the fluid flow causes the non-settling of the nanoparticles in addition to chaotic and random movement of the nanoparticles within the fluid flow. Hence, the conduction heat transfer coefficient is increased and greater convection coefficient is obtained. This result been obtained by several research groups such as Ding et al. [41] and Hay et al. [42] in their attempt to justify the increased heat transfer in the presence of nanoparticles.

In general, with the addition of nanoparticles to the base fluid, the flow structure is changed in a way that, besides increasing the thermal conductivity such as chaotic and random movements, dispersion of suspended nanoparticles leads to turbulence in the nanoparticles, and consequently the rate of energy exchange, heat transfer of the fluid and the pipe wall, and the temperature of the gas inside the pipe are increased [43, 44]. Increasing the volume concentration of nanoparticles increases the interactions and collisions between the nanoparticles.

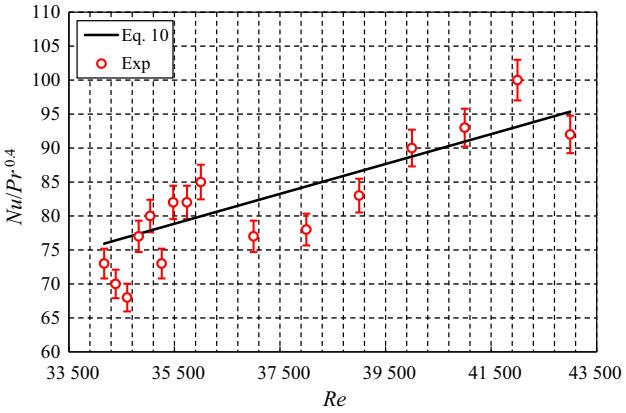

Fig. 14 $\frac{Nu}{Pr^{0.4}}$ to the Reynolds number for heating and cooling of passing air through the heat pipe

Moreover, the pump causes relative motion in the tank and the permeability of nanoparticles near the wall, leading to faster heat transfer from the nanoparticles to the wall of the pipe and air (gas) compressible fluid inside the pipe. In the other words, increasing the volume concentration of the nanoparticles intensifies the mechanisms associated with increased heat transfer in air or gas.

To calculate the convection heat coefficient, passing air or gas in laboratory devices from sweep pipes within tank, physical and thermodynamic properties and the average inlet and outlet temperatures of the laboratory indirect heater and relocation convection coefficient relations in theory and experimentally can be obtained. With increasing temperature in gases, density decreases, the viscosity coefficient increases, and the air convection coefficient increases, while with an increase in the Nusselt number, the convection coefficient increases as well. As has been shown, with an increase in the convection coefficient, the Nusselt number is also increased. According to Fig. 14 that is drawn for $\frac{Nu}{Pr^{0.4}}$ to Reynolds number Re in linear equation and with Dittos-Bolter [40] equation for the larger width of the Reynolds numbers can be used for air with $Pr = 0.72$ that with difference of 25–30% error for each of the equations and with practical Nusselt is comparable.

Experimental error

The uncertainties of the tests in the process of heat transfer are defined by experimental error, calculation error, and precision of measuring devices in line with Kolmogorov and the uncertainty standards [45, 46]. The resulting maximum error by the flow meter is ± 0.000016 m^3/s, and temperature sensors are ± 0.1 °C. The measurement temperature error, flow rate, and the measurement related to the diameter of the pipe in the heat transfer coefficient were calculated on the basis of the Kline–McClintock error

theory [47], and its maximum value was 3.22%. Regarding the random errors, errors of measurement device, and errors of heat loss from the tank to the ambience, the maximum error in the calculation of the heat transfer coefficient was equal to 19.24%.

Conclusions

In this study, temperature difference improvement in the presence of nano-copper oxide and water–ethylene glycol (50:50) has been investigated empirically in a laboratory-developed indirect heater for increasing the heat transfer and heating of cold gas (air) in the indirect heater at CGSs, thus increasing the overall heat transfer coefficients of base fluids. All these properties shrink the volume of the heater, which will be very cost-effective in the future.

On the whole, increasing nanofluids' thermal conductivity coefficient depends on the volume of the particles, size, and shape of the nanoparticles, the type of the base fluid, and the nanoparticles. Conduction and convection heat transfer coefficients can be increased significantly with the addition of small amounts of copper oxide nanoparticles to water–ethylene glycol base fluid. In the present study, as the experimental data show, the following results have been obtained at volume fractions of 0.025, 0.05, 0.1, 0.2 and 0.3, and diameter of 40 nm in temperatures of 40, 50, 60 and 70 °C:

1. We observed 36% growth as the highest temperature difference of the air outlet (gas), which is considered one of the most important parameters in volume fraction of 0.2 and temperature of 70 °C.
2. The nanofluid thermal conductivity coefficient increased to the base fluid (k^{nf}/k_{bf}) with increasing temperature and volume fraction, and in volume fraction of 0.2% and at a temperature of 70 °C, 36% more increase in air temperature (gas) output was observed in the indirect heater.
3. The ratio of theoretical Nusselt to experimental had a difference less than 30%, which was due to the absence of any effect of some physical properties on the convection heat transfer coefficient.
4. The results showed that due to prevailing operating conditions in the indirect heater system at CGSs, the use of copper oxide nanoparticles in the base fluid to create the temperature difference of 15–20 °C in the output of pipe for gas compressible fluid is very appropriate and has relatively good and satisfactory consistency with the theoretical discussions.

References

1. Kargaran M, Arabkoohsar A, Hagighat-Hosini SJ, Farzaneh-Kord V, Farzaneh-Gord M. The second law analysis of natural gas behavior within a vortex tube. Therm Sci. 2013;17(4):1079–92.
2. Farzaneh-Gord M, Hashemi S, Sadi M. Energy destruction in Iran's natural gas pipe line network. Energy Explor Exploit. 2007;25(6):393–406.
3. Farzaneh-Gord M, Sadi M. Enhancing energy output in Iran's natural gas pressure drop stations by cogeneration. J Energy Inst. 2008;81(4):191–6.
4. Choi SUS, Eastman JA. Enhancing thermal conductivity of fluids with nanoparticles, no.1 ANL/MSD/CP—84938, CONF-951135–29. Argonne National Lab., IL, USA. 1995.
5. Nadooshan AA, Esfe MH, Afrand M. Evaluation of rheological behavior of 10W40 lubricant containing hybrid nano-material by measuring dynamic viscosity. Phys E. 2017;92:47–54.
6. Toghraie D, Chaharsoghi VA, Afrand M. Measurement of thermal conductivity of ZnO–TiO2/EG hybrid nanofluid. J Therm Anal Calorim. 2016;125:527–35.
7. Hemmat Esfe M, Naderi A, Akbari M, Afrand M, Karimipour A. Evaluation of thermal conductivity of COOH-functionalized MWCNTs/water via temperature and solid volume fraction by using experimental data and ANN methods. J Therm Anal Calorim. 2015;121:1273–8.
8. Hemmat Esfe M, Saedodin S, Yan W-M, Afrand M, Sina N. Study on thermal conductivity of water-based nanofluids with hybrid suspensions of CNTs/Al2O3 nanoparticles. J Therm Anal Calorim. 2016;124:455–60.
9. Nadooshan AA. An experimental correlation approach for predicting thermal conductivity of water-EG based nanofluids of zinc oxide. Phys E Low Dimens Syst Nanostruct. 2017;87:15–9.
10. Dardan E, Afrand M, Isfahani AHM. Effect of suspending hybrid nano-additives on rheological behavior of engine oil and pumping power. Appl Therm Eng. 2016;109:524–34.
11. Goodarzi M, Kherbeet AS, Afrand M, Sadeghinezhad E, Mehrali M, Zahedi P, Wongwises S, Dahari M. Investigation of heat transfer performance and friction factor of a counter-flow double-pipe heat exchanger using nitrogen-doped, graphene-based nanofluids. Int Commun Heat Mass Transf. 2016;76:16–23.
12. Toghraie D, Mokhtari M, Afrand M. Molecular dynamic simulation of Copper and Platinum nanoparticles Poiseuille flow in a nanochannels. Phys E. 2016;84:152–61.
13. Afrand M, Najafabadi KN, Sina N, Safaei MR, Kherbeet AS, Wongwises S, Dahari M. Prediction of dynamic viscosity of a hybrid nano-lubricant by an optimal artificial neural network. Int Commun Heat Mass Transf. 2016;76:209–14.
14. Vafaei M, Afrand M, Sina N, Kalbasi R, Sourani F, Teimouri H. Evaluation of thermal conductivity of MgO-MWCNTs/EG hybrid nanofluids based on experimental data by selecting optimal artificial neural networks. Phys E. 2017;85:90–6.
15. Shamshirband S, Malvandi A, Karimipour A, Goodarzi M, Afrand M, Petković D, Dahari M, Mahmoodian N. Performance investigation of micro- and nano-sized particle erosion in a 90° elbow using an ANFIS model. Powder Technol. 2015;284:336–43.
16. Afrand M. Experimental study on thermal conductivity of ethylene glycol containing hybrid nano-additives and development of a new correlation. Appl Therm Eng. 2017;110:1111–9.
17. Afrand M, Nazari Najafabadi K, Akbari M. Effects of temperature and solid volume fraction on viscosity of SiO2-MWCNTs/SAE40 hybrid nanofluid as a coolant and lubricant in heat engines. Appl Therm Eng. 2016;102:45–54.
18. Shahsavani E, Afrand M, Kalbasi R. Experimental study on rheological behavior of water–ethylene glycol mixture in the

presence of functionalized multi-walled carbon nanotubes. J Therm Anal Calorim 1-9. https://doi.org/10.1007/s10973-017-6711-8.
19. Afrand M, Nadooshan AA, Hassani M, Yarmand H, Dahari M. Predicting the viscosity of multi-walled carbon nanotubes/water nanofluid by developing an optimal artificial neural network based on experimental data. Int Commun Heat Mass Transf. 2016;77:49–53.
20. Nadooshan, AA, Esfe MH, Afrand M. Prediction of rheological behavior of SiO2-MWCNTs/10W40 hybrid nanolubricant by designing neural network. J Therm Anal Calorim 1-8. https://doi.org/10.1007/s10973-017-6688-3.
21. Xuan Y, Li Q. Heat transfer enhancement of nanofluids. Int J Heat Fluid Flow. 2000;21(1):58–64.
22. Li Q, Xuan Y. Convective heat transfer and flow characteristics of Cu-water nanofluid. Sci China Ser E Technol Sci. 2002;45(4):408–16.
23. Farzaneh-Gord M, Arabkoohsar A, Rezaei M, Deymi-Dashte-Bayaz M, Rahbari HR. Feasibility of employing solar energy in natural gas pressure drop stations. J Energy Inst. 2011;84(3):165–73.
24. Farzaneh-Gord M, Arabkoohsar A, Dasht-bayaz MD, Farzaneh-Kord V. Feasibility of accompanying uncontrolled linear heater with solar system in natural gas pressure drop stations. Energy. 2012;41(1):420–8.
25. Farzaneh-Gord M, Arabkoohsar A, Dasht-bayaz MD, Machado L, Koury RNN. Energy and exergy analysis of natural gas pressure reduction points equipped with solar heat and controllable heaters. Renew Energy. 2014;72:258–70.
26. Behseresht A, Noghrehabadi A, Ghalambaz M. Natural-convection heat and mass transfer from a vertical cone in porous media filled with nanofluids using the practical ranges of nanofluids thermo-physical properties. Chem Eng Res Des. 2014;92(3):447–52.
27. Noghrehabadi A, Ghalambaz M, Ghanbarzadeh A. Effects of variable viscosity and thermal conductivity on natural-convection of nanofluids past a vertical plate in porous media. J Mech. 2014;30(03):265–75.
28. Hussein AM, Bakar RA, Kadirgama K, Sharma KV. Heat transfer enhancement with elliptical tube under turbulent flow TiO2-water nanofluid. Therm Sci. 2016;20(1):89–97.
29. Mehmood R, Nadeem S, Sher Akbar N. Non-aligned ethylene-glycol 30% based stagnation point fluid over a stretching surface with hematite nano particles. J Appl Fluid Mech. 2016;9:1359–66.
30. Masuda H, Ebata A, Teramae K. Alteration of thermal conductivity and viscosity of liquid by dispersing ultra-fine particles. Dispersion of Al2O3, SiO2 and TiO2 ultra-fine particles, pp. 227-233 (1993).
31. Wen D, Ding Y. Formulation of nanofluids for natural convective heat transfer applications. Int J Heat Fluid Flow. 2005;26(6):855–64.
32. Xuan Y, Roetzel W. Conceptions for heat transfer correlation of nanofluids. Int J Heat Mass Transf. 2000;43(19):3701–7.
33. Buckingham E. On physically similar systems: illustrations of the use of dimensional equations. Phys Rev. 1914;4(4):345–76.
34. Langhaar HL. Dimensional analysis and theory of models, vol. 2. New York: Wiley; 1951.
35. Handbook, ASHRAE Fundamentals. American society of heating, refrigerating and air-conditioning engineers. Atlanta: Inc.; 2009.
36. Ebrahimnia-Bajestan E, Moghadam MC, Niazmand H, Daungthongsuk W, Wongwises S. Experimental and numerical investigation of nanofluids heat transfer characteristics for application in solar heat exchangers. Int J Heat Mass Transf. 2016;92:1041–52.
37. Pak BC, Cho YI. Hydrodynamic and heat transfer study of dispersed fluids with submicron metallic oxide particles. Exp Heat Transf Int J. 1998;11(2):151–70.
38. Brinkman HC. The viscosity of concentrated suspensions and solutions. J Chem Phys. 1952;20(4):571.
39. Yu W, Choi SUS. The role of interfacial layers in the enhanced thermal conductivity of nanofluids: a renovated Maxwell model. J Nanopart Res. 2003;5(1–2):167–71.
40. Dittus FW, Boelter LMK. Heat transfer in automobile radiators of the tubular type. Int Commun Heat Mass Transf. 1985;12(1):3–22.
41. Ding Y, Alias H, Wen D, Williams RA. Heat transfer of aqueous suspensions of carbon nanotubes (CNT nanofluids). Int J Heat Mass Transf. 2006;49(1):240–50.
42. He Y, Jin Y, Chen H, Ding Y, Cang D, Huilin L. Heat transfer and flow behaviour of aqueous suspensions of TiO_2 nanoparticles (nanofluids) flowing upward through a vertical pipe. Int J Heat Mass Transf. 2007;50(11):2272–81.
43. Heris SZ, Esfahany MN, Etemad SG. Experimental investigation of convective heat transfer of Al_2O_3/water nanofluid in circular tube. Int J Heat Fluid Flow. 2007;28(2):203–10.
44. Anoop KB, Sundararajan T, Das SK. Effect of particle size on the convective heat transfer in nanofluid in the developing region. Int J Heat Mass Transf. 2009;52(9):2189–95.
45. Liu B. Fuzzy process, hybrid process and uncertain process. J Uncertain Syst. 2008;2(1):3–16.
46. Lira I. Evaluating the measurement uncertainty: fundamentals and practical guidance. Am J Phys. 2003;71:93–4.
47. Kline SJ, McClintock FA. Describing uncertainties in single-sample experiments. Mech Eng. 1953;75(1):3–8.